

# Numerical Investigation of Capabilities for Dynamic Self-Shading through Shape Changing Building Surface Tiles

**Robert Joseph Zupan<sup>1</sup>, Dale Clifford<sup>2</sup>, Richard Beblo<sup>3</sup>, John Brigham<sup>4</sup>**

- 1 University of Pittsburgh, Pittsburgh, PA, United States of America
- 2 California Polytechnic State University, San Luis Obispo, CA, United States of America
- 3 University of Dayton Research Institute, Dayton, OH, United States of America
- 4 Durham University, Durham, United Kingdom

## **Abstract**

*A concept for a smart material morphing building surface tile that would utilise adaptive surface wrinkle patterns to improve solar interaction is explored. The effect of the wrinkle patterns is numerically investigated in the context of an objective to reduce solar irradiance entering buildings by changing the shape of the surface (i.e. surface topography) so that the façade is self-shading, thereby reducing energy costs of the building for temperature control. A generally applicable algorithm was utilised, and is presented to quantify the area of an arbitrarily shaped/oriented surface that is in shade for any given date/time and geographic location. Numerical case studies are shown that utilise the self-shading algorithm to evaluate the capabilities of various wrinkle patterns, both static and dynamically changing, to self-shade a building surface over the course of a day. The results indicate that a morphing wrinkle pattern can substantially increase the amount and duration of surface area in shade over time in comparison to any static (non-morphing) patterns, although it is noted that changing the surface pattern results in a trade-off in the energy cost. Furthermore, it is shown that as the location of the proposed tile on the building changes, the optimal wrinkle pattern changes as well.*

## **Keywords**

*Morphing, Building Envelope, Self-Shading, Cactus Tile, Adaptive Structures, Wrinkle, Smart Material*

DOI: 10.7480/jfde.2018.1.1781

# 1 INTRODUCTION

Buildings that can adaptively respond to fluctuating environmental conditions have the proven potential to increase occupant comfort and significantly decrease energy consumption and carbon emissions (Hughes & Dhannu, 2008; Z. Sun, Wang, & Ma, 2011). Moreover, with commercial buildings alone accounting for over 40% of energy consumption in the United States (Energy, 2010), environmentally responsive building technologies for reducing energy consumption are a particularly promising area of collaborative and multidisciplinary research. The main consumers of energy in commercial buildings are lighting, ventilation, and heating and cooling (Energy, 2010). Therefore, in an effort to increase energy efficiency, many building technologies being developed focus on optimally regulating these main consumers using a variety of dynamic control systems for lighting (Bryans & Jump, 2001; Eckel et al., 1999; Guillemain & Morel, 2001; Hughes & Dhannu, 2008), ventilation (Ayata, Çam, & Yıldız, 2007; Gavan, Woloszyn, Kuznik, & Roux, 2010; Hagentoft, Sasic Kalagasidis, Nilsson, & Thorin, 2008; Z. Sun et al., 2011), and cooling (Aldawoud, 2013; Inoue, 2003; Ip, Lam, & Miller, 2010). These technologies are widely used in commercial buildings, and recently, in an effort to further increase energy efficiency, researchers have been focusing on utilising the building envelope (Capeluto & Ochoa, 2014; Sauchelli, Lobaccaro, Masera, & Fiorito, 2013; Zhou & Chen, 2010), which includes the façade, roof, and windows.

Technologies that utilise the building envelope, such as the façade, have been shown to affect the energy demand of commercial buildings (Chwieduk, 2003; Yan Liu et al.; Sadineni, Madala, & Boehm, 2011; Sozer, 2010). These technologies have the ability to affect ventilation, interior lighting, and wind drag by utilising varying porosity (Chang, 2006; Karava, Stathopoulos, & Athienitis, 2007), light filtering (Aldawoud, 2013), and varying surface texture (Lignarolo, Lelieveld, & Teuffel, 2011). The present work focuses on environmentally responsive exterior shading. Controlling how the building interacts with sunlight has the potential to reduce both lighting and heating and cooling costs. Examples of exterior building components that focus specifically on interaction with light that have been proposed include external louvres and awnings/overhangs (Dubois & Arch, 1998; Hashemi, 2014; Jones, 1980; Nielsen, Svendsen, & Jensen, 2011; Palmero-Marrero & Oliveira, 2010), photovoltaic panels (Di Vincenzo, Kesten, & Infield, 2010; L. Sun, Lu, & Yang, 2012; Wang & Hsu, 2010; Yoo & Manz, 2011), and building surface skins (R. M. Barrett & M. R. P. Barrett, 2016; R. M. Barrett & R. P. Barrett, 2016a, 2016b; Cilento, 2012; Dewidar, Mohamed, & Ashour, 2013; Fiorito et al., 2016; Nagy et al., 2016).

Of the adaptive building envelope technologies in existence and under development, many utilise smart materials to facilitate the adaptive behaviour. A recent example is the proposed use of hygromorphic materials to create an adaptive structure concept that is inspired by the opening and closing of the surface elements of conifer cones (Holstov, Bridgens, & Farmer, 2015). Alternatively, Barrett and co-workers (R. M. Barrett & M. R. P. Barrett, 2016; R. M. Barrett & R. P. Barrett, 2016a, 2016b) have been developing a device that is likely most similar to the concept proposed herein, in terms of both objective and mechanism. Barrett et al. have proposed a smart material building covering, called "Thermadapt", that would change shape based on thermal loading throughout the day. To achieve the surface morphing the building coverings take advantage of coefficient of thermal expansion (CTE) mismatch. The building covering has an outer layer with a lower CTE than the inner layer, therefore when the temperature rises the inner layer expands first, causing the building covering to curve outwards, altering the shape of the exterior into a self-shading configuration. The inner layer would also be the first to contract in cold weather, causing the building coverings to curve inwards, providing insulation by trapping air pockets under the coverings. This building covering technology has been shown to lead to peak temperatures 10 - 14° F lower than ambient

peak temperatures. It also performs well in cold temperatures, showing similar temperatures as standard insulation while using much less material. On a larger scale, Capeluto investigated the effects of utilising a larger portion of the building envelope for self-shading purposes and showed similar positive results (Capeluto, 2003).

This work proposes a building surface tile that (similarly to Barrett's work) self-shades the surface to affect the solar irradiance entering the building. In contrast, the approach for self-shading is based upon a technology that was previously explored by Clifford, referred to as "cactus tiles" (Carnegie Mellon University). The cactus tile is a bio-inspired form for a building surface that is based on the skin of a cactus, which has extensive wrinkling that functions to self-shade the cactus and prevent it from overheating in the sun. This effect was explored previously by Ehleringer (Ehleringer, Mooney, Gulmon, & Rundel, 1980). Preliminary tests showed that on a 100° F day on a south-facing façade, a wrinkled building surface was 30° F cooler than a surrounding unshaded brick surface, substantially lowering thermal transfer to the building interior. However, this concept was initially envisioned to be static (i.e. the wrinkle pattern of the building surface would be the same year-round), and would not account for changes in the angle/direction of sunlight or changes in the self-shading (i.e. cooling) demand throughout a day and a year. As such, the current study intends to explore the potential of a morphing cactus tile that has a dynamically changing wrinkle pattern, which could control the level of self-shading provided by the façade based on the time of day and/or season. The key difference between the proposed technology and the technologies developed by Barrett (R. M. Barrett & M. R. P. Barrett, 2016; R. M. Barrett & R. P. Barrett, 2016a, 2016b), Nagy (Nagy et al., 2016), and others is that the proposed technology has a continuous deformable surface while the others simply have discrete elements with a limited range of motion. Therefore, it is expected that the proposed technology will have a design space with a higher number of solutions, potentially leading to greater efficiency or functionality.

To evaluate the potential of this morphing cactus tile concept and to motivate future efforts to develop the technology, a set of numerical case studies were investigated regarding the self-shading capability of various static and dynamic cactus tiles surface topographies. First, it was necessary to identify and utilise an algorithm to calculate the portion of a surface that is self-shaded for any feasible (wrinkled) tile shape, geographic location, and environmental conditions, which is elaborated upon in the following. Then, the case studies are presented, which examine the potential self-shading capabilities of various basic wrinkle pattern possibilities throughout a given day. Lastly, concluding remarks and future directions to further explore the proposed technology are discussed.

An important note is that the potential benefit of having non-flat tile shapes is through the control of how heat is transferred to the building. Specifically, note the fourth-order relationship between thermal radiation and temperature in contrast to the linear relationship of thermal convection and conduction to temperature (Howell, Menguc, & Siegel, 2010). For example, if a fixed amount of solar energy is focused on a surface area that is 50% smaller than the original area of the surface, the resulting temperature of the exposed surface area will be doubled. Due to the fourth-order relationship between temperature and thermal radiation this leads to the thermal energy being radiated from the tile to increase by a factor of 16, which in turn reduces the amount of the finite thermal energy being conducted into the building. In this simplified example, radiation and convection are assumed to be wholly exterior phenomena.

## 2 ALGORITHM FOR QUANTIFICATION OF SELF-SHADING OF AN ARBITRARY SURFACE

Most applications requiring quantification of shaded area of a surface have largely focused on structured shapes, such as overhangs, awnings, and louvres (Dubois & Arch, 1998; Hashemi, 2014; Jones, 1980; Nielsen et al., 2011; Palmero-Marrero & Oliveira, 2010; Pongpattana & Rakkwamsuk, 2006; Yanda & Jones, 1983). As such, the algorithms utilised therein are not applicable to arbitrarily shaped surfaces as are considered here for the morphing building surface tile concept, and a more generalised algorithm is needed. Rendering technology, such as Radiosity (Cohen & Wallace, 2012; Hanrahan, Salzman, & Aupperle, 1991), uses algorithms capable of calculating the area of shaded area of arbitrarily shaped surfaces. Therefore, an algorithm, similar to those used in such technologies, was modified to be applicable to a shape defined by a finite element mesh.

The shading quantification algorithm utilised assumes that the surface to be evaluated be defined by a standard finite element-type mesh, based upon a set of nodes and their connectivity as elements. Then, all that is necessary is to determine the state of shading of each element, using a form of backwards ray tracing, and numerically integrate over the mesh to determine the total area that is self-shaded for the given arbitrarily shaped surface. As such, the algorithm utilised to quantify the self-shading of an arbitrary surface can be described as follows:

**INPUT:** nodal coordinates and element connectivity of mesh description of surface, latitude, longitude, and elevation of the surface location, date, and time.

- 1 Calculate Azimuth and Zenith angles of the sun's position relative to the surface (as detailed in the following).
- 2 Loop over each element in the mesh, and for each element:
  - a Determine the centroid of the element.
  - b Determine the direction (vector) of a solar ray that passes through the centroid.
  - c Determine if any other element in the mesh intersects the solar ray vector (i.e. shading the current element).
  - d If the solar ray vector intersects any other element (between current element and sun), then add the current element area to the total shaded area sum.

A critical element of any approach to shading quantification (including the algorithm utilised herein) is calculation of the solar position at the point in space and time on the surface of interest. There are numerous methods to determine solar position, characterised by the zenith (or elevation) and azimuth angles (Blanco-Muriel, Alarcón-Padilla, López-Moratalla, & Lara-Coira, 2001; Grena, 2008; Reda & Andreas, 2004). The algorithm used in the present effort is the Solar Position Algorithm (SPA) developed in Reda and Andreas (2004). SPA was chosen because of the relatively high accuracy compared to other options, with maximum uncertainties in the calculated angles of  $\pm 0.0003^\circ$ .

As detailed in Reda and Andreas (2004), SPA requires the location (latitude and longitude), date, time, and spatial and temporal properties of the location (elevation, average annual temp/pressure, etc.), and puts out several solar position measures, including those required for the self-shading quantification algorithm herein of the zenith and azimuth angles. The unit vector of the solar ray can then be characterised using the zenith and azimuth angles as:

$$v_s = \begin{bmatrix} -\cos(\gamma_s) * \cos(\alpha_s) \\ -\cos(\gamma_s) * \sin(\alpha_s) \\ \sin(\gamma_s) \end{bmatrix} \quad (1)$$

where  $\gamma_s$  is the elevation angle (degrees),  $\alpha_s$  is the azimuth angle relative to south (degrees), north is positive x, west is positive y, and height is positive z.

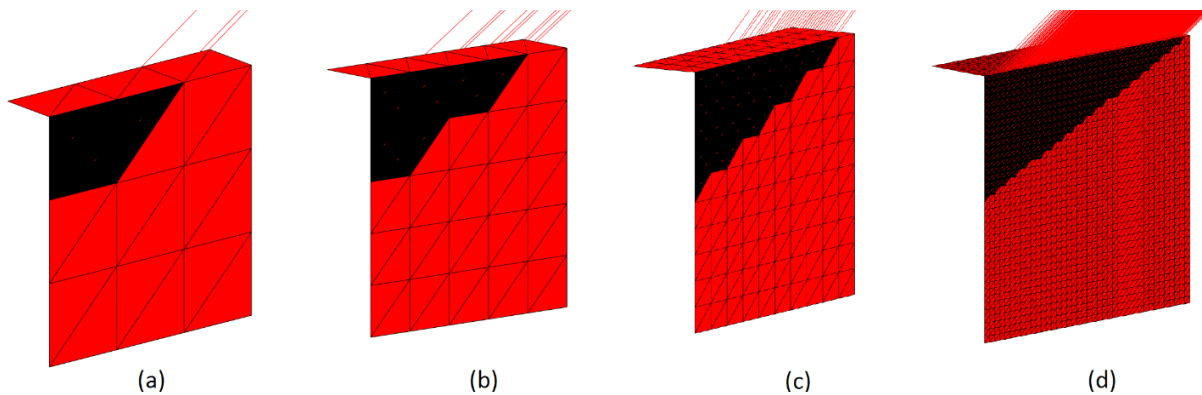


FIG. 32 Example of the self-shading estimate from the algorithm presented herein for four different levels of mesh refinement (a - d), with shaded elements in black and exposed elements in red.

A final component to an algorithm such as this is to perform a mesh convergence analysis to ensure that the mesh utilised to produce the final result is sufficiently small for the result to be accurate. As shown in Figure 1 for an example self-shading calculation, the algorithm would be repeated with sequentially more refined meshes until the shading estimate stops significantly changing. As can be seen in the example, the estimates provided by Figure 1(c) and Figure 1(d) are significantly more similar than either of the prior estimates, and it is likely that the estimate in Figure 1(d) is sufficiently converged.

To verify and validate the accuracy of the self-shading algorithm, examples of shading geometries, their locations, and orientations from Pongpattana and Rakkwamsuk (2006) were evaluated. The first shape considered was the overhang shape shown in Figure 2, oriented west at 13:07 on March 10<sup>th</sup>, 2004. The algorithm was verified by first performing a mesh dependency study, and then comparing to the analytical solution found by projecting the overhang through the solar angle onto the vertical wall and calculating the shaded area using simple geometry. The algorithm converged to a value differing from the analytical solution by 0.1% using 3584 elements, confirming the algorithm converges within acceptable limits.

Finally, to validate the present algorithm, converged estimates of surface shaded area were calculated for two additional test cases from the work in Pongpattana and Rakkwamsuk (2006) that had corresponding experimental measurements. The two test cases considered were the overhang case with the same location and orientation from the verification test and a double vertical fin device oriented west at 13:36 on March 14<sup>th</sup>, 2004, as shown in Figure 3. The experimental result reported (Pongpattana & Rakkwamsuk, 2006) for the overhang case was 75% shaded area, in contrast to the 73% predicted by the shading quantification algorithm. Additionally, the shading quantification algorithm estimated a self-shaded area of 17% for the conditions of the double vertical fin case, while the experimental results were 19%. With both sample cases resulting in differences between the experimental and numerical estimates of shading of only 2%, the shading quantification algorithm was considered to have calculated the shaded area of the objects within acceptable limits.

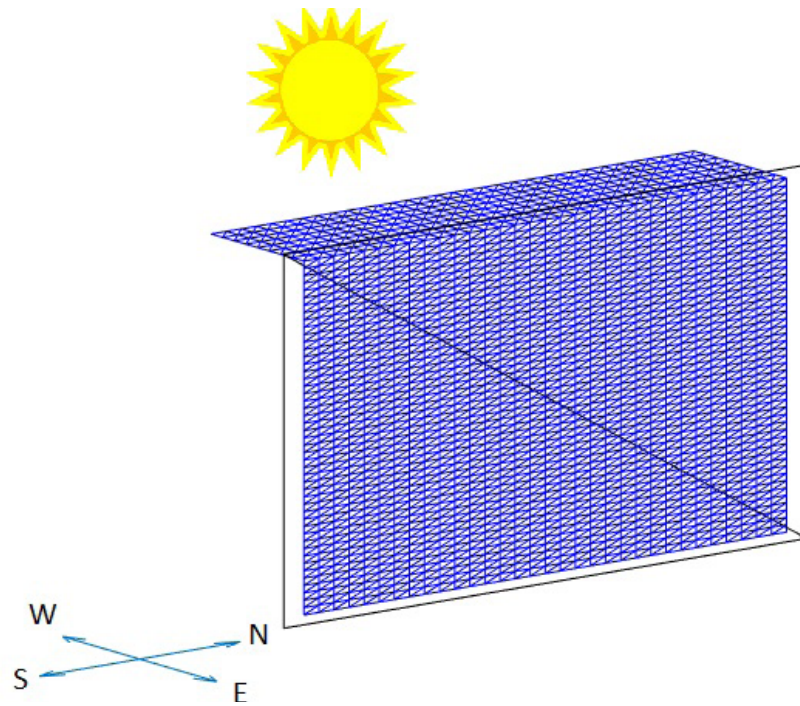


FIG. 33 Meshed representation of the west-facing overhang surface example.

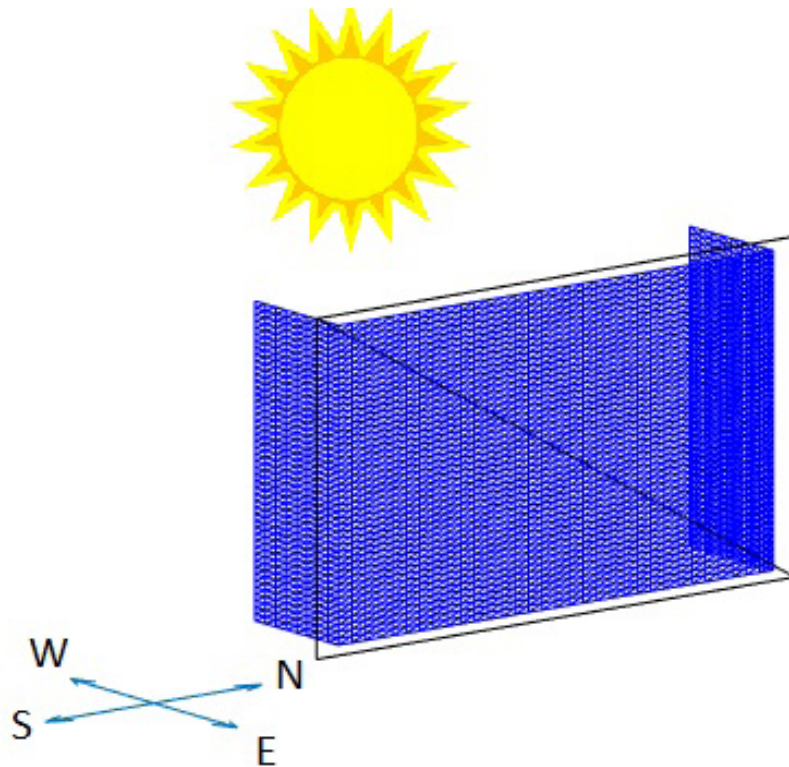


FIG. 34 Mesh representation of the double vertical fin surface example.

### 3 SELF-SHADING NUMERICAL CASE STUDIES

Several case studies were numerically investigated with respect to shading potential of the proposed building surface tile concept involving various scenarios for potential tile shapes, orientation, location, and time of day. Overall, these case studies were based upon a single shape-changing tile, covering a 1m by 1m plane area, on a conceptual surface located in Phoenix, Arizona (Lat: 33.45, Long: -112.07) throughout the day of July 4<sup>th</sup>, 2015. It was assumed that the tile would be rigidly held on two of the four edges (e.g., top and bottom or left and right), and with shape changing only occurring through changes in the out-of-plane surface position. It was further assumed that the tile would operate similarly to the previously mentioned technology being developed by Barrett et al. (R. M. Barrett & M. R. P. Barrett, 2016; R. M. Barrett & R. P. Barrett, 2016a, 2016b), with the tile being comprised of a smart material, and the shape change therefore being achieved by deformation of the tile material (rather than mechanical components such as hinges). To address potential material limitations at this stage of the development (i.e. without having selected an optimal smart material for device construction), each shape change considered was normalised for comparability between shapes such that the surface area change with respect to a flat surface was fixed at 150% (i.e. the total surface area of each deformed shape considered was fixed at 1.5 m<sup>2</sup>). Although the distribution of this deformation would likely become important in future development, this 150% overall deformation is well within the limits of many smart materials, such as shape memory polymers (Mather, Luo, & Rousseau, 2009) (commonly shown to exceed 200% recoverable deformation). Furthermore, the normalisation allows each shape change to be fairly compared in the sense that the total deformation is equivalent.

For simplicity, three basic wrinkle patterns were considered, which were chosen somewhat arbitrarily, but based upon the previously discussed concept of a “cactus” tile (Carnegie Mellon University). The three basic wrinkle patterns considered (in addition to the undeformed tile) are shown in Figure 4, and are described by the equation for the out-of-plane surface position,  $z$ , as

a single sin-wave overhang:

$$z = \begin{cases} A * \left[ \sin\left(\frac{2*\pi}{P} * \left(x + \frac{3*P}{4}\right)\right) + 1 \right] & \text{for } 0 \leq x \leq 4 - P \\ 0 & \text{for } 4 - P < x \leq 4 \end{cases}, \quad (2)$$

a continuous unidirectional sin-wave:

$$z = A - \frac{A}{2} * \left[ \sin\left(\frac{2*\pi}{P} * \left(x + \frac{3*P}{4}\right)\right) + 1 \right] \quad \text{for } 0 \leq x \leq 4. \quad (3)$$

and a continuous bidirectional sin-wave:

$$z = A - \frac{A}{2} * \left[ \cos\left(\frac{2*\pi}{P} * (x - 4)\right) + \cos\left(\frac{2*\pi}{P} * (y - 4)\right) \right] \quad \text{for } 0 \leq x, y \leq 4 \quad (4)$$

where  $x$  and  $y$  are the in-plane coordinates of the plate, and  $A$  and  $P$  are the amplitude and period of the sin-wave, respectively.

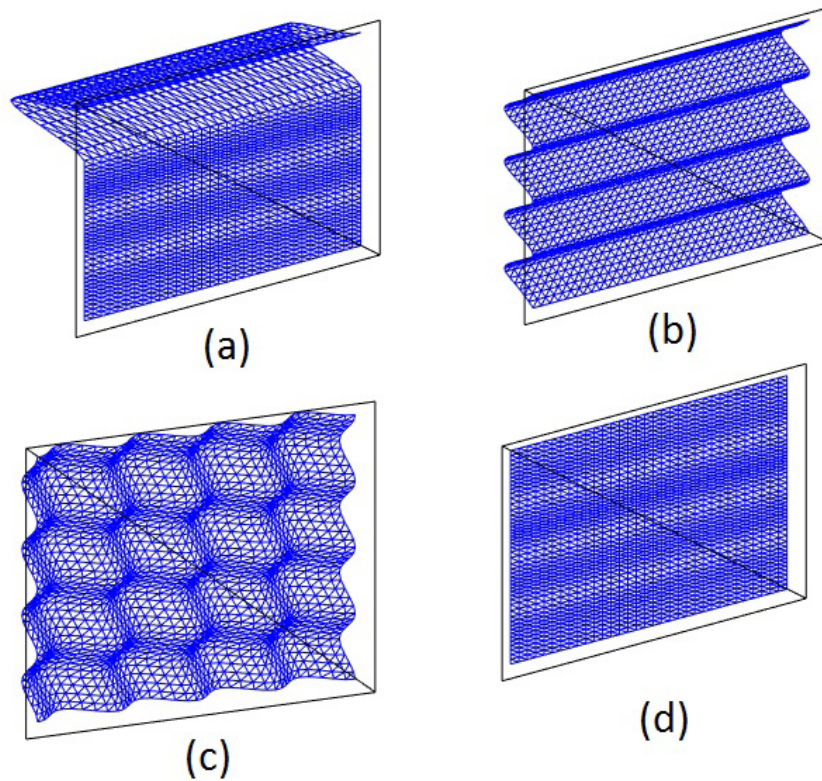


FIG. 35 Mesh-based surface representation of the (a) single sin-wave overhang, (b) continuous unidirectional sin-wave, (c) continuous bidirectional sin-wave, (d) undeformed tile shapes

To quantify the shading potential of each tile scenario over time, the 10-hour period of daylight on the specified date was considered and the surface shading for each tile scenario was calculated each hour on the hour for two conceptual locations on the building, a west-facing vertical wall and a south-facing roof (45°). In the following, the self-shading potential of these three basic wrinkle patterns is examined individually by evaluating the amount of self-shading for a set of variations (e.g., changes in shape amplitude, etc.) for each basic shape form over the specified 10-hour period. Next, the basic wrinkle patterns are compared to one another in terms of the shading capability. An important note is that this first set of tests considered the tiles to be static (i.e. non-morphing) to evaluate the potential of the shapes. Next, the potential self-shading of a morphing tile is evaluated by considering the capability of the tile to morph between the wrinkle patterns, and considering both shading throughout the day as well as a measure of complexity for the morphing process. Finally, a comparison is made between the results of the two conceptual locations on the building. It should be noted that mesh convergence was confirmed for all shapes.

### 3.1 SHADING POTENTIAL OF THE INDIVIDUAL BASIC WRINKLE PATTERNS

The percentage of each tile shaded was determined over the specified day for three variations of each shape form for the vertical west wall. The variations in the three basic wrinkle patterns were generated by modifying the values of A and P in (2), (3), and (4). Table 1 shows all nine parameter combinations of the basic wrinkle patterns considered. Again, note that the shape variations all maintained the specified total surface area constraint (i.e. increasing the period of the shapes required increasing the amplitude to maintain the 1.5 m<sup>2</sup> surface area).

Figure 5 compares the percentage of the tile surface area shaded over time for the variations considered for the overhang basic shape form. The overhang with a period of 0.125 m provides the highest percentage of self-shading until approximately 13:30, then the overhang with a period of 0.250 m temporarily provides the highest shading until approximately 14:30. The overhang with a period of 0.500 m provides the highest percentage from 14:30 to 17:00, at which point the periods of 0.125 m and 0.250 m provide approximately equivalent shading for the remainder of the day. Figure 6 shows the analogous results for the unidirectional sin-wave. The unidirectional sin-wave with period of 0.125 m provides the highest percentage of self-shading for the entirety of the day except between 15:00 and 16:00 hours, when the period of 0.250 m temporarily provides more shading. Finally, Figure 7 shows the percentage of the tile shaded over time for the three different parameter combinations of the bidirectional sin-wave shape. Similar to the unidirectional sin-wave, the period of 0.125 m provides the highest self-shading for the first part of the day, until approximately 15:30, and once again the three shape variations remain approximately equivalent for the remainder of the day. Generally, as the period decreased (i.e. the more “wrinkly” the shapes became) the amount of self-shading increased. However, with the limitation on the total surface area, there is a point of diminishing returns when decreasing the period size (which increases the number of shadows), since the amplitude must correspondingly decrease (which decreases each shadow height). Although not shown here for brevity, additional tests indicated that this point of diminishing returns was approximately the amplitude of 0.125 m for the examples herein.

Shape:	P (m)	A (m)
Overhang	0.125	0.1550
	0.250	0.1740
	0.500	0.2150
Unidirectional Sin-wave	0.125	0.0342
	0.250	0.0675
	0.500	0.1350
Bidirectional Sin-wave	0.125	0.0975
	0.250	0.1850
	0.500	0.3656

TABLE 18 The period (P) and amplitude (A) for each of the variations of the wrinkle patterns considered.

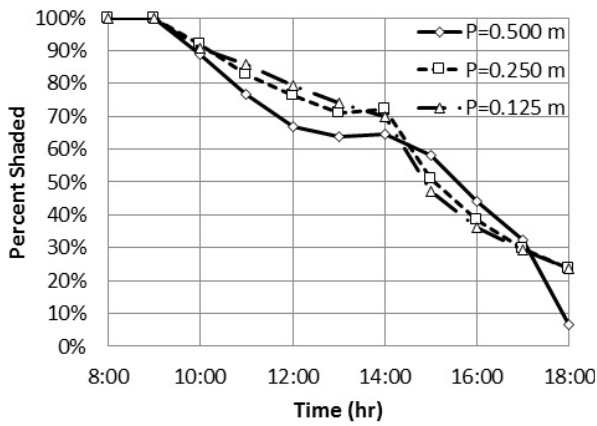


FIG. 36 Percentage of the surface that is self-shaded with respect to the time of day for variations of the period length (P) of the single sin-wave overhang shape.

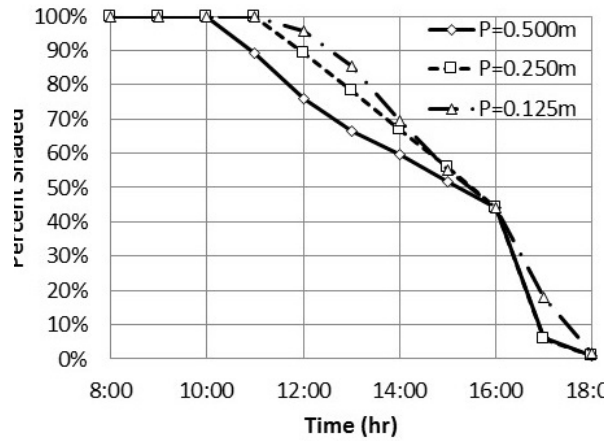


FIG. 37 Percentage of the surface that is self-shaded with respect to the time of day for variations of the period (P) of the unidirectional sin-wave shape.

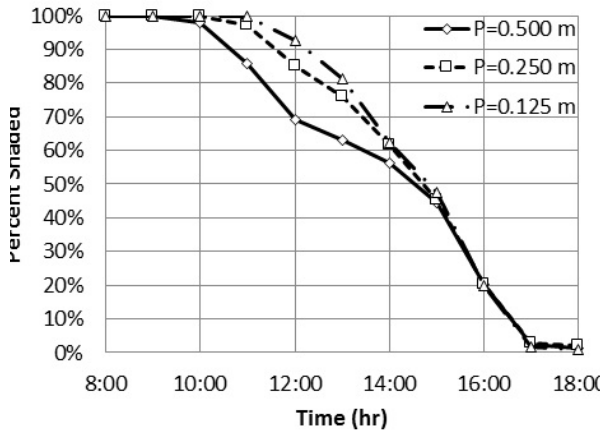


FIG. 38 Percentage of the surface that is self-shaded with respect to the time of day for variations of the period length (P) of the bidirectional sin-wave shape.

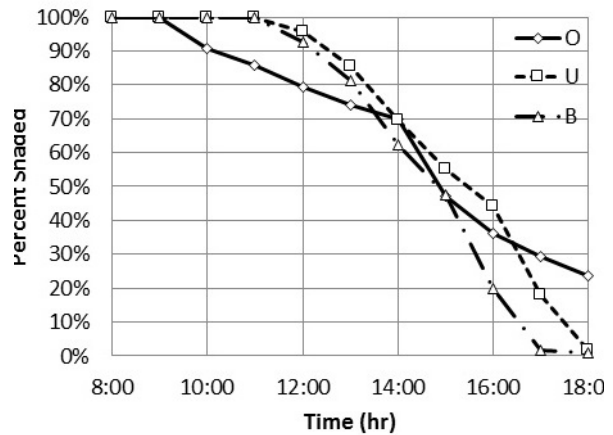


FIG. 39 Percentage of the surface that is self-shaded with respect to time of day for the overhang (O), unidirectional (U), and bidirectional (B) shapes with period length of 0.125m.

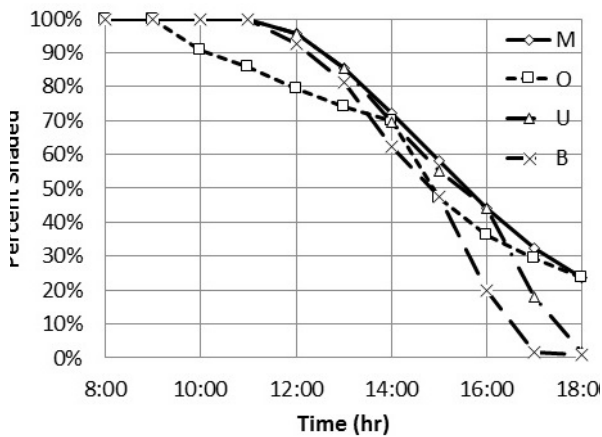


FIG. 40 Percentage of the surface that is self-shaded with respect to time of day for a morphing tile (M) and the overhang (O), unidirectional (U), and bidirectional (B) shapes with period length of 0.125m.

Figure 8 shows the shading over time for the three basic wrinkle patterns with a period of 0.125 m (i.e. the period with the highest total shading over the day for each). The unidirectional sin-wave had the highest percentage of shading for a large portion of the day, with the exception of 14:00 and after 16:30 when the overhang shape provided the highest amount of self-shading. More importantly, a general observation from Figures 5-8 is that none of the basic wrinkle patterns or parameter combinations had a higher amount of self-shading than the others throughout the entirety of the day. In other words, a tile that is able to morph between such shapes and parameter combinations throughout the day would be able to self-shade more of the surface over a longer period of time compared to any static shape considered.

### 3.2 SHADING POTENTIAL OF A DYNAMIC TILE SHAPE

To begin evaluation of the potential of a morphing tile, Figure 9 shows the optimal combination of the shapes considered in the previous section in terms of maximising the total shaded area over the day by allowing the tile shape to change every hour compared to the highest total shading static versions (i.e. unchanging) of the basic wrinkle patterns. The morphing tile shades the surface significantly more over the day than any one of the static shapes, with a total percentage of surface-hours of shade (i.e. area under the shaded percentage vs. time curve) of 7.50 compared to the next highest static shape, the unidirectional sin-wave of 7.18. However, an important aspect that has not been discussed up to this point is that there is expected to be an energy (or other) cost to morph a surface tile from one shape to another. Therefore, the optimised morphing process shown in Figure 9, which requires five shape changes, may ultimately have more cost than benefit compared to a tile that changes shape less often in certain circumstances.

Again, it should be noted that without further developments of the proposed technology the morphing cost cannot be predicted precisely. Depending on the smart material/structure mechanism used, this cost could include energy for activation or actuation of the structure/material or simply the complexity of the build needed to achieve the functionality. To provide a perspective, it is assumed herein that the cost of performing a shape change is directly proportional to a measure of the difference between the two subsequent tile shapes during the morphing process. Again, noting that the hypothetical mechanism for the morphing tiles herein would be deformation (as through the use of a smart material), the amount of deformation (i.e. shape change) is expected to be a reasonable estimate of the relative input energy required to morph. As such, the following metric of the difference between two tile shapes was utilised:

$$D_{i,j} = \left( \int_0^4 \int_0^4 (z_i - z_j)^2 dx dy \right)^{1/2} \quad (5)$$

where  $z_i$  and  $z_j$  are the out-of-plane surface positions of the shapes at the  $i^{\text{th}}$  and  $j^{\text{th}}$  hour, respectively. The difference metrics for all possible combinations of the shapes considered are displayed in Table 2.

		Overhang			Unidirectional Sin-wave			Bidirectional Sin-wave		
	Period (m)	P = 0.125	P = 0.250	P = 0.500	P = 0.125	P = 0.250	P = 0.500	P = 0.125	P = 0.250	P = 0.500
Overhang	P = 0.125	0.00	7.01	7.41	4.64	5.40	5.36	5.37	4.93	4.71
	P = 0.250		0.00	6.23	5.82	4.50	2.98	4.41	3.18	5.41
	P = 0.500			0.00	5.75	1.73	5.71	2.30	5.14	5.53
Unidirectional	P = 0.125				0.00	3.07	1.52	3.82	1.78	0.43
	P = 0.250					0.00	2.98	1.56	2.61	2.88
	P = 0.500						0.00	3.51	0.79	1.32
Bidirectional	P = 0.125							0.00	2.99	3.55
	P = 0.250								0.00	1.51
	P = 0.500									0.00

TABLE 19 Difference metric, calculated from (5), for each combination of shapes considered in the case studies. Note: the matrix presented in this table is symmetrical.

Considering both maximisation of the percentage of self-shading and minimisation of the cost of morphing over an entire day, selecting the optimal morphing tile can now be thought of as a multi-objective design problem as follows:

$$\text{Minimise: } B^{-1} + \beta * C \quad (6)$$

with

$$B = \int_{8:00}^{18:00} S(t)dt \quad (7)$$

and

$$C = \sum_{i=1}^{10} D_{i,i+1} \quad (8)$$

where  $S(t)$  is the percentage of shading over time and  $\beta$  is a user-defined parameter to weigh the relative importance of the two competing objectives.

To interpret the trade-off between  $B^{-1}$  and  $C$  of this morphing tile, the Pareto front was generated for the present example by varying the total number of shape changes over the day (and thus controlling the morphing cost). Figure 10(a) shows the value of the two design objectives for each point on the Pareto front and Figure 10(b) shows the corresponding sequence of shapes obtained from the shading maximisation. The Pareto front shows that there is a substantial trade-off between the morphing cost (i.e. amount of shape change) and the amount of self-shading provided throughout the day. In particular, there is a nearly linear trade-off between the cost-benefit of 0 to 3 shape changes over the day (especially 1 to 3 shape changes). Alternatively, the increase in the amount of shading decreases significantly after 3 shape changes, with almost negligible differences in the total shading with 3 shape changes compared to 5 shape changes, but with a substantial increase in the shape change cost. An important reminder, however, is that this design solution set is for one particular tile location/position on a conceptual building, and it is expected that not only different geographic locations, but even different positions on the same building would yield different optimal morphing tile systems, as considered in the following.

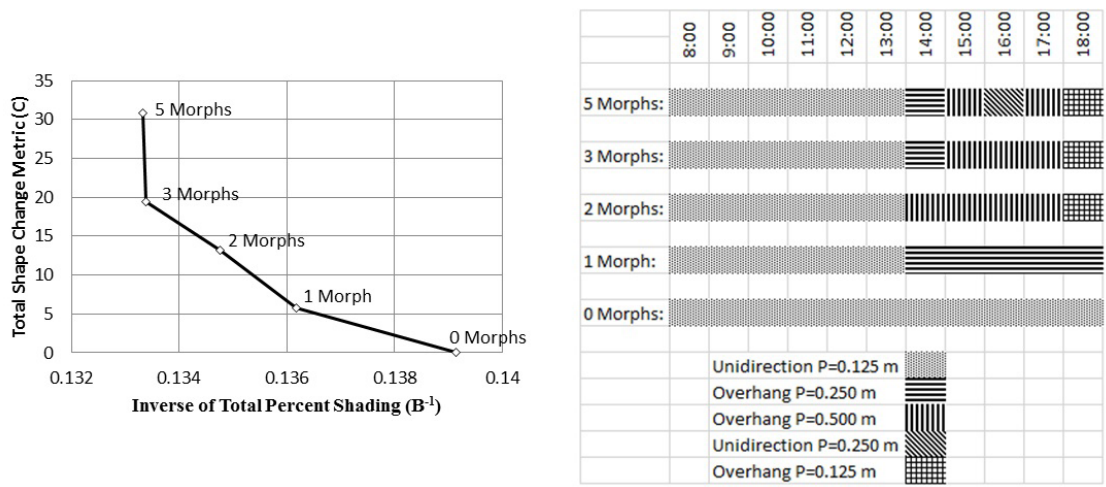


FIG. 41 (a) The total shape change metric (B) with respect to the inverse of the total percentage of shading over the day (A) and (b) the sequence of shapes for each point on the morphing tile Pareto front.

### 3.3 SHADING POTENTIAL FOR A DIFFERENT MORPHING TILE LOCATION

To evaluate how a tile's location on the façade might affect the morphing scheme, an additional set of numerical tests were carried out. This second set of tests considered a tile at the same geographic location and date as the previous tests, but on a south-facing roof façade angled at 45° (in contrast to the west-facing vertical wall considered previously). For the roof façade, the self-shading throughout the day was calculated for the same basic wrinkle patterns (and variations) that were previously considered. Additionally, for this roof example, each shape form and period variation was considered with the entire surface rotated in plane by 90°. Note that these 90° variations were also tested for the wall example, but not shown/discussed previously since they were all considerably less effective in self-shading the surfaces compared to the original orientations (which is a relatively intuitive result based on the expected path of the sun with respect to a west-facing vertical surface).

Figure 11 shows the percentage of self-shading with respect to time for the optimal variation (i.e. period value and rotation producing the highest total shading) of the three basic shapes on the roof façade. There are significant differences between the self-shading provided by each shape (and parameter variation) for the roof example compared to the wall. First, while the period of 0.125 m provided the most self-shading for all shapes on the wall, the period of 0.500 m provided the most self-shading for the overhang shape on the roof. In addition, the change in the percentage of shading over time for each shape (i.e. the shading curve) is substantially different for the roof compared to the wall, with the beginning of the day having considerably more differences between the shapes for the roof case. Also of note is the fact that the original orientations overall provided higher shading compared to their 90° rotation counterparts, but the 90° rotations provided the highest self-shading at specific hours. In particular, the bidirectional sin-wave shape had the highest amount of self-shading at both the beginning and end of the day for the roof, when considering no rotation, but never had the highest self-shading for the vertical wall. The total percentage of surface-hours of shade was also much higher for the bidirectional sin-wave shape, indicating that it provides a higher shading on average.

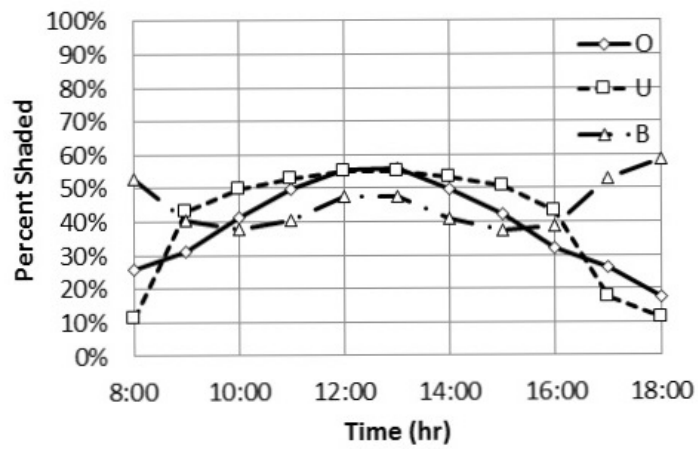


FIG. 42 Percentage of the surface that is self-shaded with respect to time of day for the overhang shape with period of 0.500 m (O), the unidirectional shape with period of 0.125 m (U), and the bidirectional shape with period of 0.125 m (B), all with the original orientation.

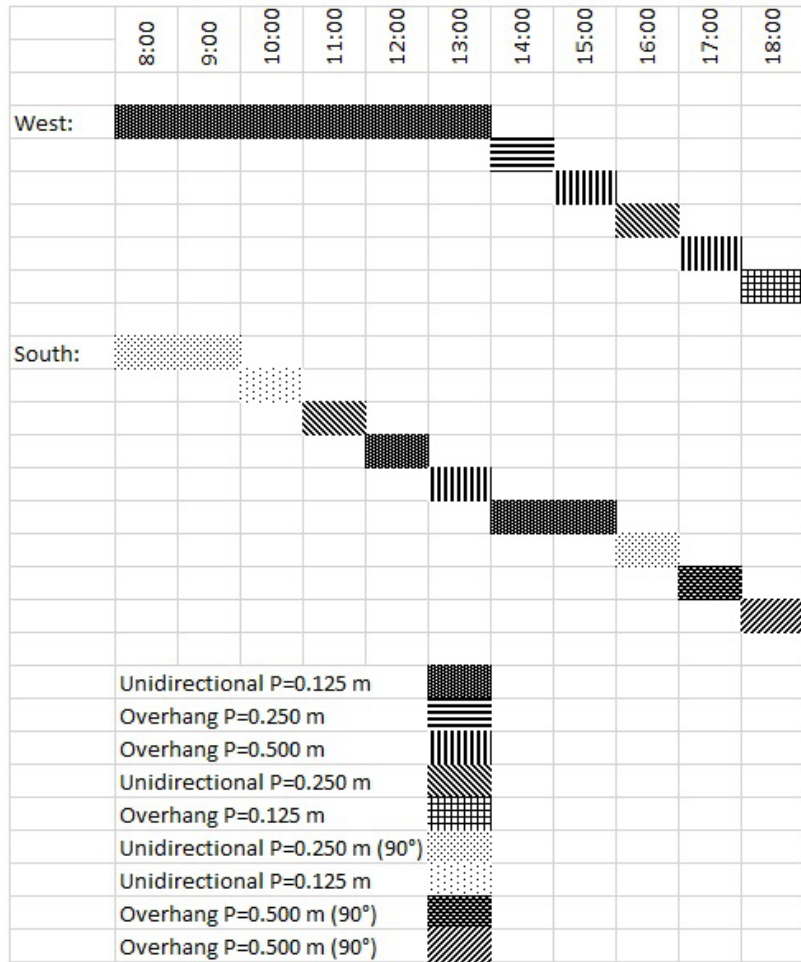


FIG. 43 Gantt chart representing the shape sequences for the west wall and south roof façades that maximise the total self-shading over the day. (It should be noted that shapes that were not optimal at any times are not taken into account in the legend.)

To further compare the two building locations, Figure 12 shows the combination of the shapes that maximises the total shaded area over the day by allowing the tile shape to change every hour (not considering the cost of the shape changes) for the roof example compared to the analogous combination previously shown for the wall example. In particular, the optimal combination for the roof was considerably more dynamic, with eight shape changes between seven shape variations, which is a change almost every hour, compared to just five changes between five variations for the wall. In addition, maximising the self-shading through morphing had a significantly larger effect on the roof, with the optimised shape change sequence yielding 5.47 total percentage of surface-hours of shade, which is 24.6% greater than the highest value for any of the static shapes, compared to the 4.5% increase provided by morphing for the wall. It should be noted that even though the bidirectional sin-wave was the best static shape in terms of total percentage of surface-hours of shade, it never provided the highest self-shading of all variations considered at any specific hour, so it does not appear in Figure 12. If there was a limitation on the number of morphs, the bidirectional sin-wave would most likely be in the optimal scheme.

## 4 CONCLUSIONS AND FUTURE DIRECTIONS

A concept was presented and numerically investigated for a morphing building tile that would reduce solar irradiance entering buildings by changing the surface topography so that the building envelope is self-shading, thereby reducing energy used by internal temperature control. Numerical case studies were used to evaluate the capabilities of this concept with three basic wrinkle patterns, both static and dynamically changing, to self-shade a building surface over the course of a day. The results indicated that a morphing surface can provide an increase in the total percentage of surface hours of shade as large as 24.6%, in comparison to the highest performing static (non-morphing) shapes. However, it was noted that there is an expected trade-off in the mechanical cost to change the surface topography. For example, it is expected that there will be a point in the design where the increase in self-shading from further morphing will not be worth the energy required to achieve morphing (e.g. through material activation and/or mechanical actuation if using a smart material component). In particular, the results showed a substantial reduction in the improvement to the self-shading after three shape changes for the designs considered. Yet, a significant change in self-shading behaviour depending upon the tile location was observed, in terms of both total shading capability and the benefits of morphing. Therefore, separate design optimisations, such as that presented, would likely be beneficial for tiles that would be located in different geographic locations and positions/orientations on the building surface.

Although the results presented show promise for a morphing, self-shading tile technology to significantly improve solar interaction for a building envelope, there are several considerations moving forward with development. One critical consideration is the full effect that this technology will have on the energy demand of a building. This physical process needs further investigation to truly understand the potential of the technology proposed herein and those that are similar. Another consideration is the choice/development of a smart material solution out of the multitude of existing concepts to facilitate the controllable surface topography. For example, two smart materials that are potentially applicable are shape memory alloys (SMAs) (Duerig, Melton, & Stöckel, 2013; Fremont, 1996; Jani, Leary, Subic, & Gibson, 2014; Morgan, 2004) and shape memory polymers (Dietsch & Tong, 2007; Lendlein & Kelch, 2002; Yanju Liu, Du, Liu, & Leng, 2014; Mather et al., 2009). Both SMAs and SMPs allow for large strain, which is expected to be a requirement of this morphing tile concept. Also, the shape memory effect of both SMAs and SMPs could aid in achieving different tile configurations

with a reduced actuation requirement. Another consideration is that throughout the presented work the design only considered a finite number of tile topographies. As such, future work to explore not only optimisation of the morphing scheme, but also the surface topography of the tile could lead to improvements to both efficiency and effectiveness.

## Acknowledgements

The authors gratefully acknowledge the financial support of the National Science Foundation through Award No. 1536797.

## References

- Aldawoud, A. (2013). Conventional fixed shading devices in comparison to an electrochromic glazing system in hot, dry climate. *Energy and Buildings*, 59, 104-110.
- Ayata, T., Çam, E., & Yildiz, O. (2007). Adaptive neuro-fuzzy inference systems (ANFIS) application to investigate potential use of natural ventilation in new building designs in Turkey. *Energy Conversion and Management*, 48(5), 1472-1479.
- Barrett, R. M., & Barrett, M. R. P. (2016). *Thermally Adaptive Building Coverings: Theory and Application*. Paper presented at the ASME 2016 Conference on Smart Materials, Adaptive Structures and Intelligent Systems.
- Barrett, R. M., & Barrett, R. P. (2016a). Thermally adaptive building covering field test. *Procedia Engineering*, 145, 26-33.
- Barrett, R. M., & Barrett, R. P. (2016b). *Thermally Adaptive Building Coverings Inspired by Botanical Thermotropism*. Paper presented at the Proceedings of the ASME 2016 Conference on Smart Materials, Adaptive Structures and Intelligent Systems (SMASIS).
- Blanco-Muriel, M., Alarcón-Padilla, D. C., López-Moratalla, T., & Lara-Coira, M. (2001). Computing the solar vector. *Solar Energy*, 70(5), 431-441.
- Bryans, D. J., & Jump, L. B. (2001). Lighting control subsystem for use in system architecture for automated building: Google Patents.
- Capeluto, I. G. (2003). Energy performance of the self-shading building envelope. *Energy and Buildings*, 35(3), 327-336.
- Capeluto, I. G., & Ochoa, C. E. (2014). Simulation-based method to determine climatic energy strategies of an adaptable building retrofit façade system. *Energy*, 76, 375-384.
- Carnegie Mellon University. Thermal Masonry. Retrieved November 6<sup>th</sup>, 2017, from <https://cmubiologic.weebly.com/cactus-tile.html>
- Chang, W. (2006). Effect of porous hedge on cross ventilation of a residential building. *Building and Environment*, 41(5), 549-556.
- Chwieduk, D. (2003). Towards sustainable-energy buildings. *Applied Energy*, 76(1), 211-217.
- Cilento, K. (2012). Al Bahar Towers Responsive Façade/Aedas. *ArchDaily*; September, 5.
- Cohen, M. F., & Wallace, J. R. (2012). *Radiosity and realistic image synthesis*: Elsevier.
- Dewidar, Y., Mohamed, N., & Ashour, Y. (2013). *Living Skins: A New Concept of Self Active Building Envelope Regulating Systems*. Paper presented at the Advancing the Green Agenda: Technology, Practices and Policies Conference-BUID.
- Di Vincenzo, M. C., Kesten, D., & Infield, D. (2010). *Assessment of performance of building shading device with integrated photovoltaics in different urban scenarios*. Paper presented at the Sustainable Energy Technologies (ICSET), 2010 IEEE International Conference on.
- Dietsch, B., & Tong, T. (2007). A review: Features and benefits of shape memory polymers (smmps). *Journal of Advanced Materials*, 39(2), 3-12.
- Dubois, M.-C., & Arch, M. (1998). *Awnings and Solar Protective Glazing for Efficient Energy Use in Cold Climates*. Paper presented at the Renewable Energy Technologies in Cold Climates' 98 Conference, May.
- Duerig, T. W., Melton, K., & Stöckel, D. (2013). *Engineering aspects of shape memory alloys*: Butterworth-Heinemann.
- Eckel, D. P., Batko, T. J., Walter, M. R., Rose, W. J., Donlon, B. P., & Zeichner, D. A. (1999). Motion sensing system with adaptive timing for controlling lighting fixtures: Google Patents.
- Ehleringer, J., Mooney, H., Gulmon, S., & Rundel, P. (1980). Orientation and its consequences for Copiapoa (Cactaceae) in the Atacama Desert. *Oecologia*, 46(1), 63-67.
- Energy, R. (2010). Energy efficiency trends in residential and commercial buildings.
- Fiorito, F., Sauchelli, M., Arroyo, D., Pesenti, M., Imperadori, M., Masera, G., & Ranzi, G. (2016). Shape morphing solar shadings: A review. *Renewable and Sustainable Energy Reviews*, 55, 863-884.
- Fremont, M. (1996). Shape memory alloy *Shape memory alloys* (pp. 1-68): Springer.
- Gavan, V., Woloszyn, M., Kuznik, F., & Roux, J.-J. (2010). Experimental study of a mechanically ventilated double-skin façade with venetian sun-shading device: A full-scale investigation in controlled environment. *Solar Energy*, 84(2), 183-195.
- Grena, R. (2008). An algorithm for the computation of the solar position. *Solar Energy*, 82(5), 462-470.
- Guillemin, A., & Morel, N. (2001). An innovative lighting controller integrated in a self-adaptive building control system. *Energy and Buildings*, 33(5), 477-487.
- Hagentoft, C.-E., Sasic Kalagasidis, A., Nilsson, S., & Thorin, M. (2008). *Mould growth control in cold attics through adaptive ventilation*. Paper presented at the Proceedings of the 8<sup>th</sup> Symposium on Building Physics in the Nordic Countries, Copenhagen Denmark.

- Hanrahan, P., Salzman, D., & Aupperle, L. (1991). *A rapid hierarchical radiosity algorithm*. Paper presented at the ACM SIGGRAPH Computer Graphics.
- Hashemi, A. (2014). Daylighting and solar shading performances of an innovative automated reflective louvre system. *Energy and Buildings*, 82, 607-620.
- Holstov, A., Bridgens, B., & Farmer, G. (2015). Hygromorphic materials for sustainable responsive architecture. *Construction and Building Materials*, 98, 570-582.
- Howell, J. R., Menguc, M. P., & Siegel, R. (2010). *Thermal radiation heat transfer*: CRC press.
- Hughes, R. F., & Dhannu, S. S. (2008). *Substantial energy savings through adaptive lighting*. Paper presented at the Electric Power Conference, 2008. EPEC 2008. IEEE Canada.
- Inoue, T. (2003). Solar shading and daylighting by means of autonomous responsive dimming glass: practical application. *Energy and Buildings*, 35(5), 463-471.
- Ip, K., Lam, M., & Miller, A. (2010). Shading performance of a vertical deciduous climbing plant canopy. *Building and Environment*, 45(1), 81-88.
- Jani, J. M., Leary, M., Subic, A., & Gibson, M. A. (2014). A review of shape memory alloy research, applications and opportunities. *Materials & Design*, 56, 1078-1113.
- Jones, R. E. (1980). Effects of overhang shading of windows having arbitrary azimuth. *Solar Energy*, 24(3), 305-312.
- Karava, P., Stathopoulos, T., & Athienitis, A. K. (2007). Wind-induced natural ventilation analysis. *Solar Energy*, 81(1), 20-30.
- Lendlein, A., & Kelch, S. (2002). Shape-memory polymers. *Angewandte Chemie International Edition*, 41(12), 2034-2057.
- Lignarolo, L., Lelieveld, C., & Teuffel, P. (2011). *Shape morphing wind-responsive facade systems realized with smart materials*. Paper presented at the Adaptive Architecture: An International Conference, London, UK, March 3-5, 2011.
- Liu, Y., Du, H., Liu, L., & Leng, J. (2014). Shape memory polymers and their composites in aerospace applications: a review. *Smart Materials and Structures*, 23(2), 023001.
- Liu, Y., Liu, J., Yang, L., Hou, L., Wang, M., & Qiao, Y. Cooling Effect for Integrated Application of Phase Change Envelopes and Night Natural Ventilation in Western China.
- Mather, P. T., Luo, X., & Rousseau, I. A. (2009). Shape memory polymer research. *Annual Review of Materials Research*, 39, 445-471.
- Morgan, N. (2004). Medical shape memory alloy applications—the market and its products. *Materials Science and Engineering: A*, 378(1), 16-23.
- Nagy, Z., Svetozarevic, B., Jayathissa, P., Begle, M., Hofer, J., Lydon, G., . . . Schlueter, A. (2016). The adaptive solar facade: from concept to prototypes. *Frontiers of Architectural Research*, 5(2), 143-156.
- Nielsen, M. V., Svendsen, S., & Jensen, L. B. (2011). Quantifying the potential of automated dynamic solar shading in office buildings through integrated simulations of energy and daylight. *Solar Energy*, 85(5), 757-768.
- Palmero-Marrero, A. I., & Oliveira, A. C. (2010). Effect of louvre shading devices on building energy requirements. *Applied Energy*, 87(6), 2040-2049.
- Pongpattana, C., & Rakkwamsuk, P. (2006). Efficient algorithm and computing tool for shading calculation. *Songklanakarin Journal of Science and Technology*, 28(2), 375-386.
- Reda, I., & Andreas, A. (2004). Solar position algorithm for solar radiation applications. *Solar Energy*, 76(5), 577-589.
- Sadineni, S. B., Madala, S., & Boehm, R. F. (2011). Passive building energy savings: A review of building envelope components. *Renewable and Sustainable Energy Reviews*, 15(8), 3617-3631.
- Sauchelli, M., Lobaccaro, G., Masera, G., & Fiorito, F. (2013). *Smart Solutions for Solar Adaptive Façade Preliminary studies for an innovative shading device*. Paper presented at the XIX IAHS World Congress., Milan, Italy.
- Sozer, H. (2010). Improving energy efficiency through the design of the building envelope. *Building and Environment*, 45(12), 2581-2593.
- Sun, L., Lu, L., & Yang, H. (2012). Optimum design of shading-type building-integrated photovoltaic claddings with different surface azimuth angles. *Applied Energy*, 90(1), 233-240.
- Sun, Z., Wang, S., & Ma, Z. (2011). In-situ implementation and validation of a CO<sub>2</sub>-based adaptive demand-controlled ventilation strategy in a multi-zone office building. *Building and Environment*, 46(1), 124-133.
- Wang, Y.-J., & Hsu, P.-C. (2010). Analytical modelling of partial shading and different orientation of photovoltaic modules. *IET Renewable Power Generation*, 4(3), 272-282.
- Yanda, R., & Jones, R. (1983). Shading effects of finite width overhang on windows facing toward the equator. *Solar Energy*, 30(2), 171-180.
- Yoo, S.-H., & Manz, H. (2011). Available remodeling simulation for a BIPV as a shading device. *Solar Energy Materials and Solar Cells*, 95(1), 394-397.
- Zhou, J., & Chen, Y. (2010). A review on applying ventilated double-skin facade to buildings in hot-summer and cold-winter zone in China. *Renewable and Sustainable Energy Reviews*, 14(4), 1321-1328.